Supplementary Information (SI) for Journal of Materials Chemistry A.
This journal is © The Royal Society of Chemistry 2024

Supporting information

Novel Two-Dimensional Conductive Metal-organic Framework based Heterostructures for High-Performance Electro-Ionic Soft Actuators

Contents

Materials and Methods

1. Materials

All chemicals and solvents were purchased from commercial sources and used without further purification. Zinc oxide (ZnO) and 1-Ethyl-3-methylimidazolium tetrafluoroborate (EMIM-BF_4) were purchased from Aladdin Reagent Co., Ltd, China. Sodium hydroxide (NaOH), N,N-dimethylacetamide (DMAC), N,N-Dimethylformamide (DMF), Acetonitrile (CH_3CN) and acetylene black were purchased from Sinopharm Chemical Reagent Co., Ltd, China. Ethanol (≥99.8%) and Acetone (≥99.8%) were purchased from JingXie High-tech Electronic Materials Co., LTD. 2,3,6,7,10,11-hexahydroxytriphenylene (HHTP) ligand was purchased from J&K Scientific, China. Polyvinylidene difluoride (PVDF, Mn 1,000,000) was purchased from Arkema, Franch. Poly(3,4-ethylenedioxythiophene)-poly(styrenesulfonate) (4.0% *wt*, PP) was purchased from Titan, China. All aqueous solutions were prepared using deionized Milli-Q water with a resistivity of 18.2 MΩ cm^{-1} at 25 °C.

2. Experiments

2.1 Synthesis of ZnO@Zn-CAT powder

A hydrothermal method was followed for the synthesis of ZnO@Zn-CAT. In nitially, the 5 mM zinc oxide (ZnO), 0.5 mM 2,3,6,7,10,11-hexahydroxytriphenylene (HHTP) ligand, and 10 mM sodium hydroxide (NaOH) was homogenously dispersed into 400 mL of deionized water under ultrasonication for 30 min. Subsequently, the vessel was sealed and heated in the oven at 85 ℃ with various growth times. After naturally cooling down to room temperature within 2 h, the dark blue mixtures, ZnO@Zn-CAT, were yielded. The isolated mixtures were further washed with 10 mM NaOH and concentrated acetone, each with vigorous stirring overnight. The mixture was washed 3 times by adding acetone, alone with centrifugation at 12000 rpm for

15 min for each cycle. The activation of as-synthesized ZnO@Zn-CAT was achieved by evacuating at 70 ℃ overnight to remove the residual solvent and store in a N_2-filled glove box at 4 ℃ until use.

2.2 Fabrication of ZnO/@Zn-CAT/PP electrodes

The fabrication of electroactive soft actuators using the nanoscale active materials Zn-CAT was performed for the first time. For the fabrication of sandwiched structures of ionic soft actuators, an homogeneous dispersion of ZnO@Zn-CAT powder (5.6 mg/mL), N,N-dimethylacetamide (DMAC) (36.4% *vol*, sonication for 30 min) and 1-Ethyl-3-methylimidazolium tetrafluoroborate (EMIM-BF_4, 0.1 g/mL) was added in Poly(3,4-ethylenedioxythiophene)-poly(styrenesulfonate) (4.0% *wt* PP, 0.64 mg/mL,) solution. The entire electrode mixture was stirred overnight at room temperature to ensure that the ZnO/Zn-CAT was uniformly distributed throughout the PP solution and could reach the most favorable level of interaction among themselves. The electrode membrane was peeled off by direct drop costed the 4 mL ZnO@Zn-CAT/PP mixture solution on a glass mode and then dried at 70 °C for 15 h.

2.3 Fabrication of EMIM-BF_4/PVDF ionic liquid gels electrolyte.

The electrolyte membrane was fabricated in a typical procedure: 1.0 g of Poly(vinylidene fluoride) (PVDF) was dissolved in 30 mL of N,N-Dimethylformamide (DMF) and subjected to stirring overnight. Subsequently, 1.5 g of EMIM-BF_4 ionic liquid was introduced into the PVDF solution, and continuous stirring was maintained for a duration of 12 h. The electrolyte membrane of the ionic liquid (IL) gels was created by directly casting the EMIM-BF_4/PVDF IL gels electrolyte onto a glass mold, followed by drying at a temperature of 70 °C for a duration of 12 h. Finally, the resulting electrolyte membrane was peeled off from the mold and used as prepared.

2.4 Fabrication of electro-active soft actuator.

The ZnO@Zn-CAT/PP electrochemical actuators were created by using a hot-

press process at 110 °C for 120 s to mechanically laminate an EMIM-BF_4/PVDF IL gels electrolyte layer with two pieces of ZnO@Zn-CAT/PP electrode layers.

3. Characterization

3.1 Material characterization

The surface morphology of the nanomaterials powder and membrane was characterized by cold field emission scanning electron microscope (FE-SEM, Hitachi-Regulus 8230) with implemented energy-dispersive X-ray spectroscopy (EDX, Oxford Aztec X-max 80 SDD EDX detector). High-resolution transmission electron microscopy (HR-TEM) and selected-area electron diffraction (SAED) patterns were performed on a FEI model Tecnai G2 F20 S-TWIN microscope. Powder X-ray diffraction (PXRD) patterns of ZnO/Zn-CAT powder were carried out using a Bruker AXS D8 Advance with filtered Cu-Kα radiation (40 kV and 40 mA, λ = 1.54056 Å) at a 2θ range of 3° to 55° with a scanning step size of 0.02° in air at room temperature. X-ray photoelectron spectra (XPS) were collected with the PHI 5000 Versaprobe II XPS Spectrometer in Nano-X Vacuum Interconnected Workstation of Suzhou Institute of Nano-Tech and Nano-Bionics (SINANO), Chinese Academy of Sciences (CAS). The Raman spectra were obtained at room temperature under a He-Cd Laser with an excitation wavelength at 523 nm (Edinburgh FLS980 spectrometer, United Kingdom). Fourier-transform infrared (FT-IR) spectra were performed by using a Thermo Nicolet iS5 in 0.8wn spectrometers instrument in the range of 500-4000 cm^{-1}. The surface areas were assessed by N_2 adsorption at 77 K using a TGA/DSC 3+ Mettler Toledo Switzerland and the samples were degassed at 100 °C under vacuum (10-5 mbar) for 12 h before analysis. The pore size distribution was calculated from the adsorption isotherms using the Barrett–Joyner–Halenda (BJH) method in the same pressure range.

3.2 Electrochemical characterization

Cyclic voltammetry (CV), electrochemical impedance spectroscopy (EIS) and Galvanostatic charge-discharge (GCD) were performed using an electrochemical workstation (CH instrument, 660E). A standard three-electrode electrochemical cell configuration (Ag/AgCl electrode as reference and platinum electrode as counter) was used to record the CV and EIS responses of the active material (ZnO@Zn-CAT) in a 3 M KOH reaction electrolyte. In the active materials measuring processes, Zn-CAT (80% *wt*), acetylene black (10% *wt*), 5% PVDF (10% *wt*) were dispersed in DMAC (0.12 g) through sonication. As-prepared ZnO@Zn-CAT paste was a bladed coating on the nickel foam at 70 °C for 12 h as the working electrode (the effective area of nickel foam is around 0.64 cm^2, mass loading is about 4.0 mg). Similarly, CV, EIS, and GCD response of PP and ZnO@Zn-CAT/PP electrodes were measured by using the standard three-electrode electrochemical cell configuration (Ag/AgCl electrode as reference and platinum electrode as counter) in a nonaqueous solution of EMIM-BF_4 (0.5 M, CH_3CN).

The potential ranges of CV testing were chosen to avoid hydrogen evolution at low potentials and the oxidation of MOF at high potentials. CV data were recorded in the potential range of 0.2 to 0.6 V of active materials ZnO@Zn-CAT and 0 to 0.8 V of ZnO@Zn-CAT/PP electrodes (versus Hg/HgO) at various scan rates ranging from 5 to 150 $mV \cdot s^{-1}$. EIS measurements were carried out in the frequency range of 100 KHz-0.01 Hz at an open-circuit potential under an AC 10 mV perturbation. GCD was performed within the voltage window of 0-0.5 V versus Hg/HgO at different current densities. The specific capacitance was calculated from CV curves according to the following equations:

$$C_{mp} = \frac{1}{2\Delta V v m} \int_{V_1}^{V_2} I dV \qquad \text{(Eq.S1)}$$

$$C_{sp} = \frac{1}{2\Delta V v S} \int_{V_1}^{V_2} I dV \qquad \text{(Eq.S2)}$$

where, ΔV (V) is the operating potential window, v (V s^{-1}) is the applied scan rate, m (g) and S (cm^{-2}) is the mass and the area of active material and electrodes, and I

(A) is the response current of CV.

4. Measurement of actuation performance

The actuation performance was applied by square-wave voltages to the actuators using a waveform generator (Tektronix, AFG 2021) under an ambient laboratory atmosphere with a 40±5% relative humidity. The free displacement (δ) from an end fixed point was continuously monitored from one side of the actuator using a vertically placed laser displacement sensor (Keyence, LK-H052) with a time interval of 10 ms, which was transformed into the strain. The strain (ε) and stress (σ) generated in the actuators were estimated by the following equations.

$$\varepsilon = \frac{2\delta d}{l^2 + d^2} \quad \text{(Eq.S3)}$$

$$\sigma = \varepsilon Y \quad \text{(Eq.S4)}$$

where δ (m), l (m), d (m), and Y (m) are the tip displacement, the free length, the thickness (m), and the Young's modulus (Pa) of the actuator, respectively.

Energy transduction efficiency (η) of the actuator was calculated according to the Eq.S5,

$$\eta_{transduction} = \frac{P_{mechanical}}{P_{input}} = \frac{0.5Y\varepsilon^2 f \cdot Vol}{IV} \quad \text{(Eq.S5)}$$

where $P_{mechanical}$ (W) and P_{input} (W) are the input electric energy and output mechanical energy of the actuator, respectively. I (A) and V (V) are the current and voltage applied on the actuator, Y (Pa), ε, f (Hz), and Vol (m^3) are the Young's modulus, strain, voltage frequency, and volume of the actuator, respectively.

5. Measurement of light-enhanced actuation performance

The light sources were selected under similar powers but different wavelengths (λ) of light (P ≈ 5 mW cm^{-2}, λ = 365, 420, 450, 500, 600, 700, and 800 nm). $\Delta Displacement$

is used to show the amount of displacement enhancement of the light-enhanced actuator under different light sources:

$$\Delta Displacement = \frac{D_L - D_A}{D_A} \quad \text{(Eq.S6)}$$

where D_L and D_A stand for the actuator displacement under light exposure and air with the excitation of input AC voltage of 3 V at 0.1 H_Z, respectively.

Under photo-thermal conversion efficiency testing, the actuator was placed at a distance of 1.5 cm away from the light source, while the temperature variation was monitored by a thermal camera (Fotric 348+#L25).

Results and Discussion

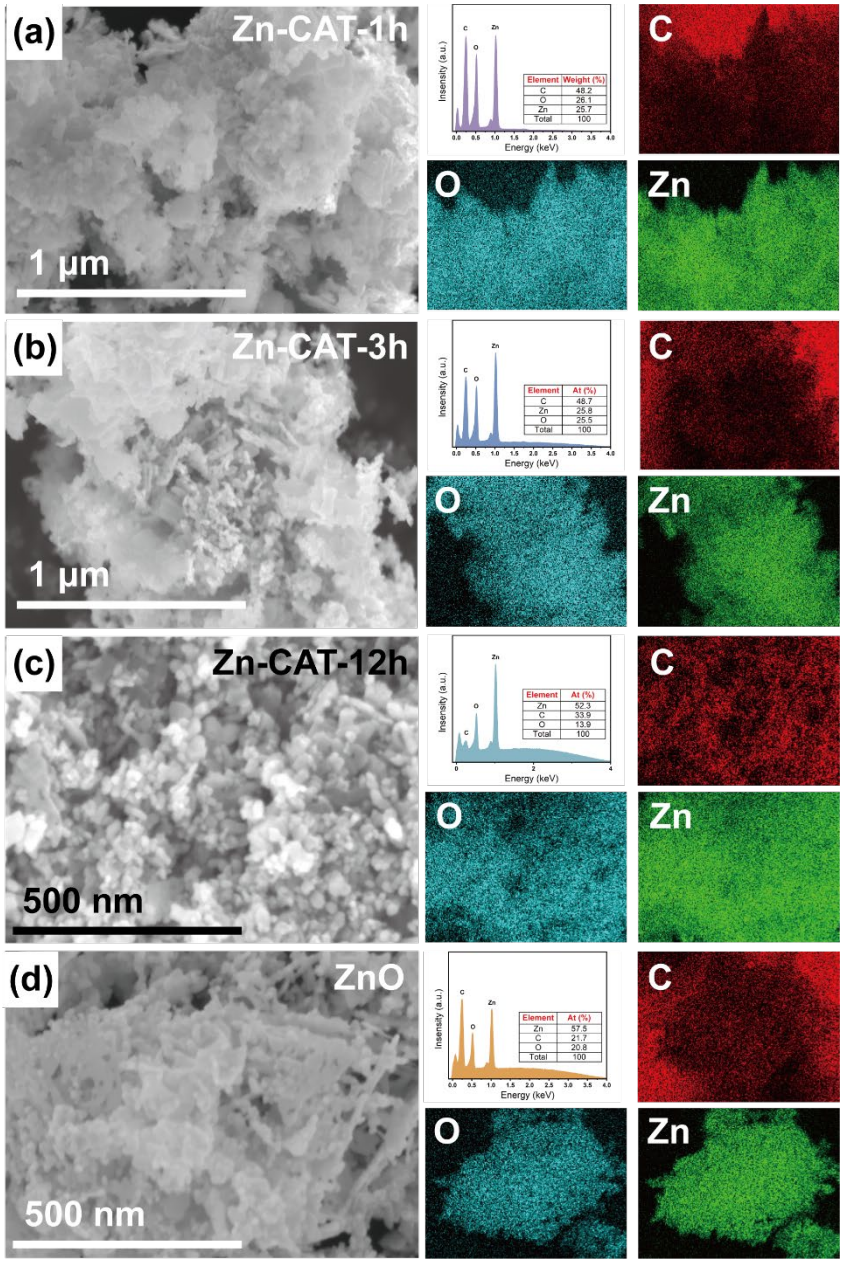

Figure S1. The SEM images of ZnO@Zn-CAT-1 (a), ZnO@Zn-CAT-3 (b), ZnO@Zn-CAT-12 (c) and ZnO (d) with corresponding EDS mapping.

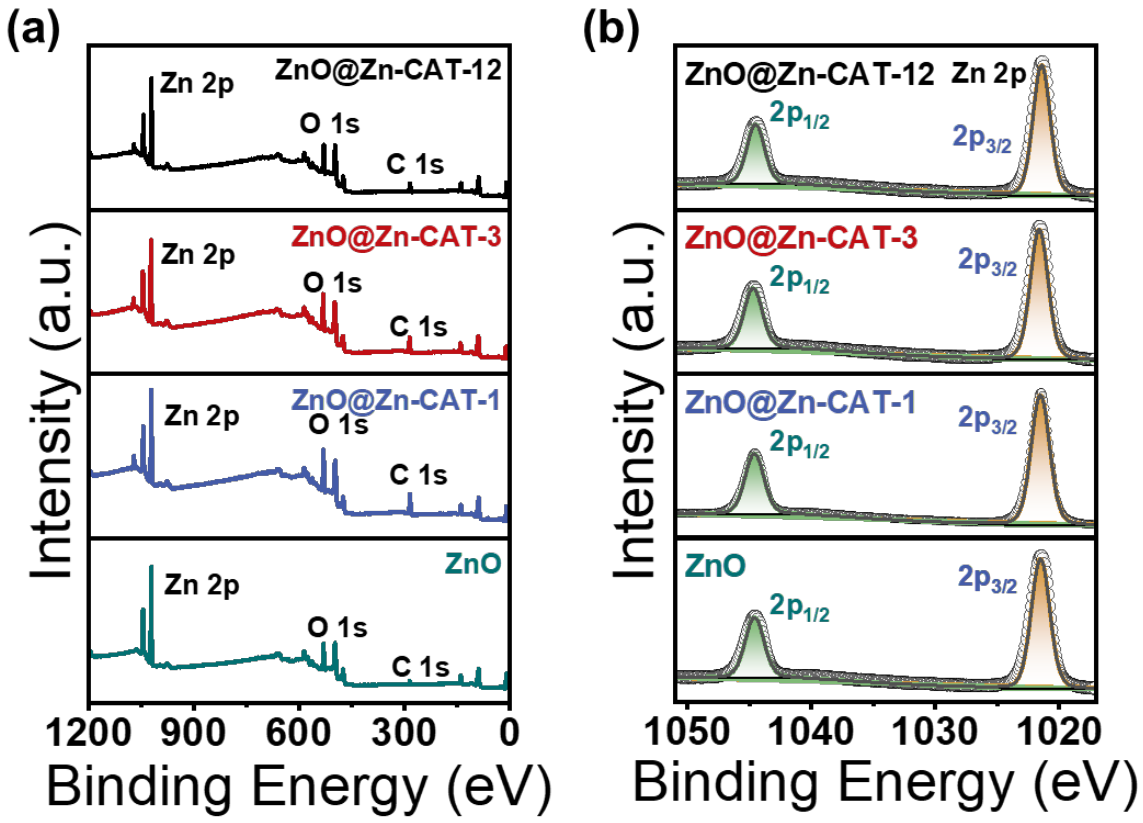

Figure S2. The XPS survey spectrum (a) and Zn 2p spectrum (b) of ZnO, ZnO@Zn-CAT-1, ZnO@Zn-CAT-3, and ZnO@Zn-CAT-12.

Table S1. Percentage of C 1s XPS spectra under different growth times.

Growth time	C=C	C-C	C-O	C=O	π-π*
1h	8.31	67.18	7.95	18.91	2.65
3h	9.34	62.03	6.58	21.60	0.45
12h	4.98	67.20	9.21	18.61	0.00

Table S2. Percentage of O 1s XPS spectra under different growth times.

Growth time	C-O	C=O	H_2O	π-π*
1h	34.01	45.11	14.65	6.24
3h	33.6	46.41	15.47	4.52
12h	35.44	50.33	10.88	3.35

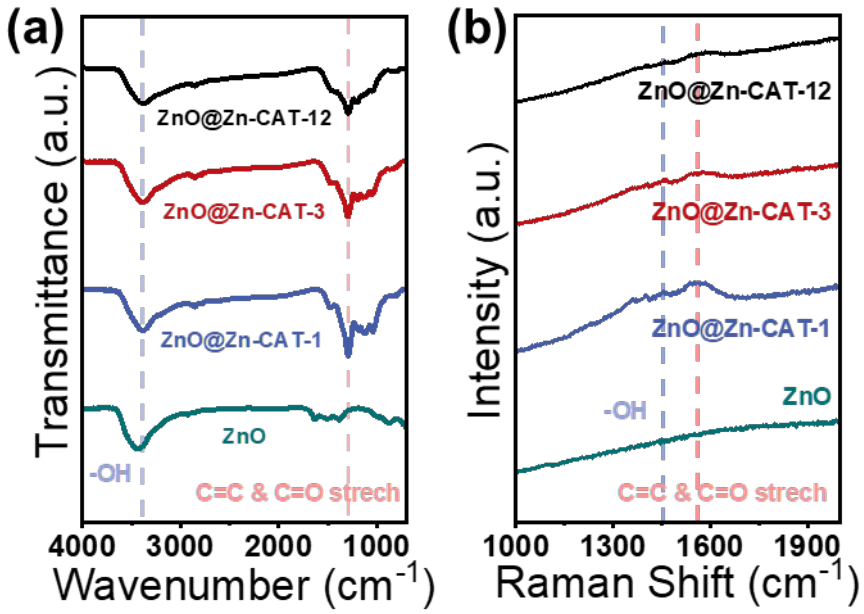

Figure S3. The FT-IR (a) and Raman (b) spectra of ZnO, ZnO@Zn-CAT-1, ZnO@Zn-CAT-3, and ZnO@Zn-CAT-12.

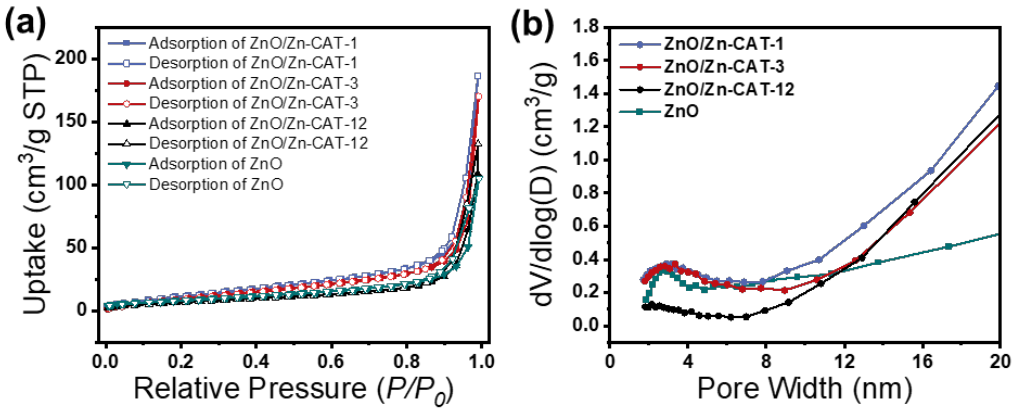

Figure S4. The nitrogen physisorption isotherms (a) and pore size distribution (b) of ZnO, ZnO@Zn-CAT-1, ZnO@Zn-CAT-3, and ZnO@Zn-CAT-12 composites.

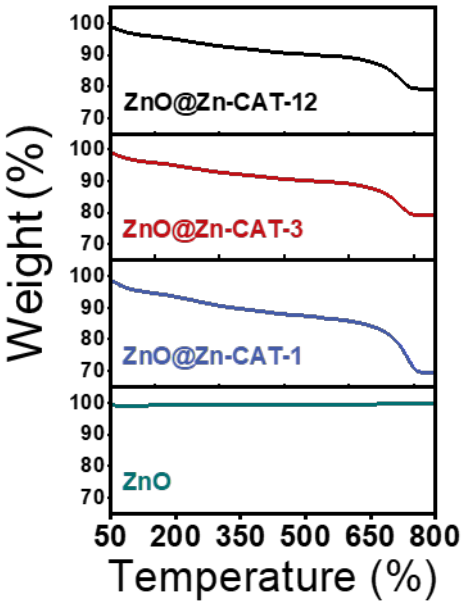

Figure S5. The thermogravimetric (TG) spectra of ZnO, ZnO@Zn-CAT-1, ZnO@Zn-CAT-3, and ZnO@Zn-CAT-12 composites up to the temperature of 1000 °C.

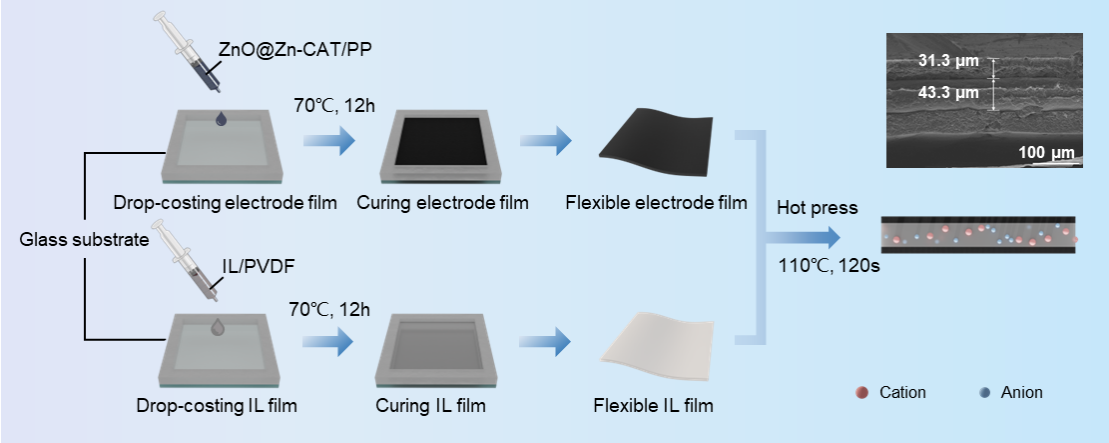

Figure S6. The schematic of the assembly procedure of the ZnO@Zn-CAT actuator and cross-sectional SEM image.

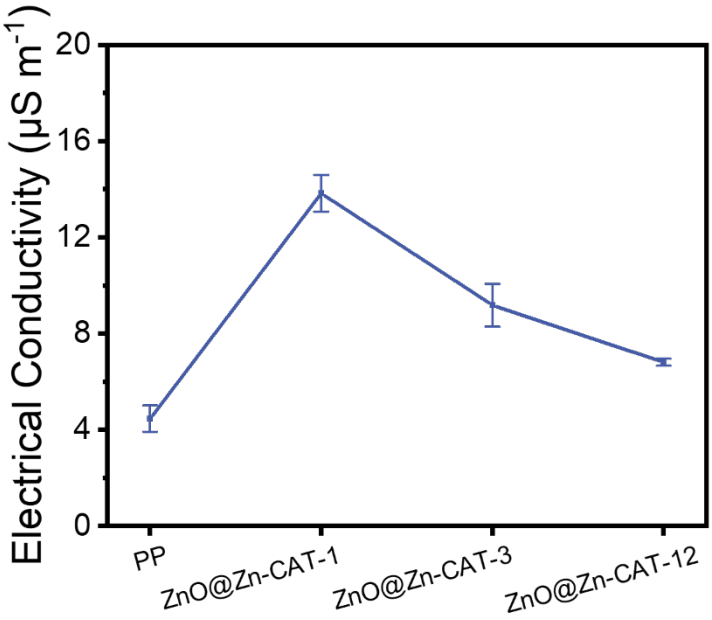

Figure S7. The electrical conductivity of all electrode films.

Table S3. Statistical data on the dimensions and performance of soft actuators.

Property		Average (mm)
Length		1.0
Thickness	IL film	0.0433
	Single electrode	0.0313
	Total	0.1059
Width		0.5

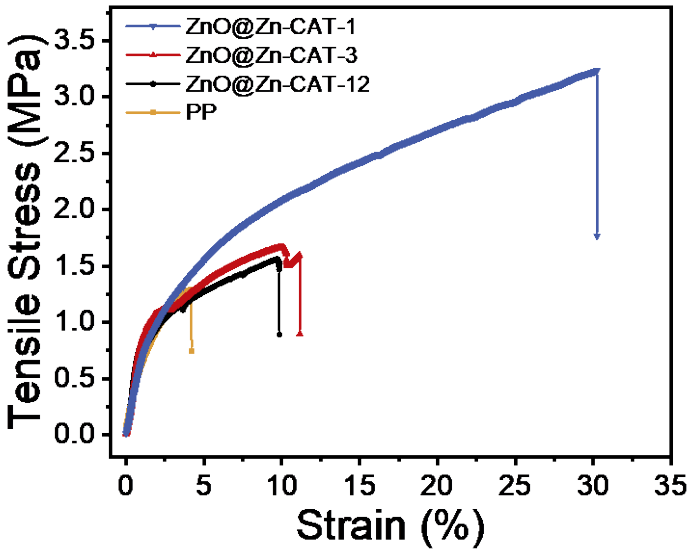

Figure S8. The stress-strain curves of PP, ZnO@Zn-CAT-1, ZnO@Zn-CAT-3, and ZnO@Zn-CAT-12 based actuators.

Table S4. Mechanical properties of the actuators.

Property	**PP soft actuator**	**ZnO@Zn-CAT-1 soft actuator**	**ZnO@Zn-CAT-3 soft actuator**	**ZnO@Zn-CAT-12 soft actuator**
Tensile strength (MPa)	1.28	3.23	1.66	1.56
Young's modulus (MPa)	63.0	70.10	87.0	88.0

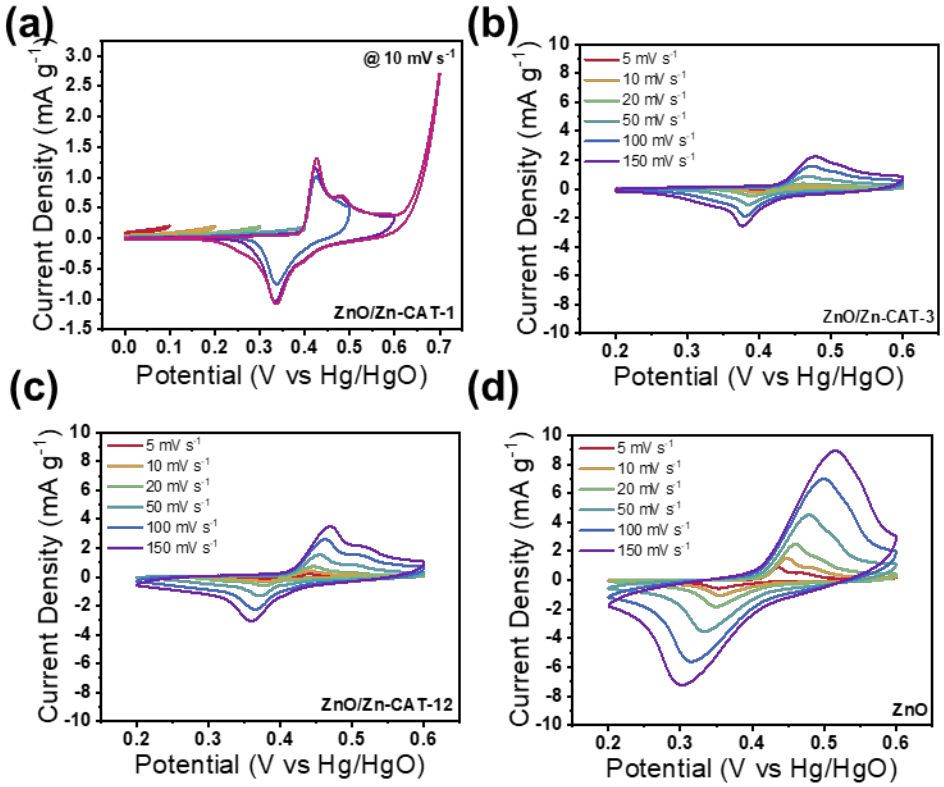

Figure S9. (a) The cyclic voltammetry curves of ZnO@Zn-CAT powder with increasing potential limits in the positive direction at a sweep rate of 10 mV s^{-1}. The CV curves of (b) ZnO@Zn-CAT-3, (c) ZnO@Zn-CAT-3, and (d) pure ZnO composite at scan rates from 5 to 200 mV s^{-1}.

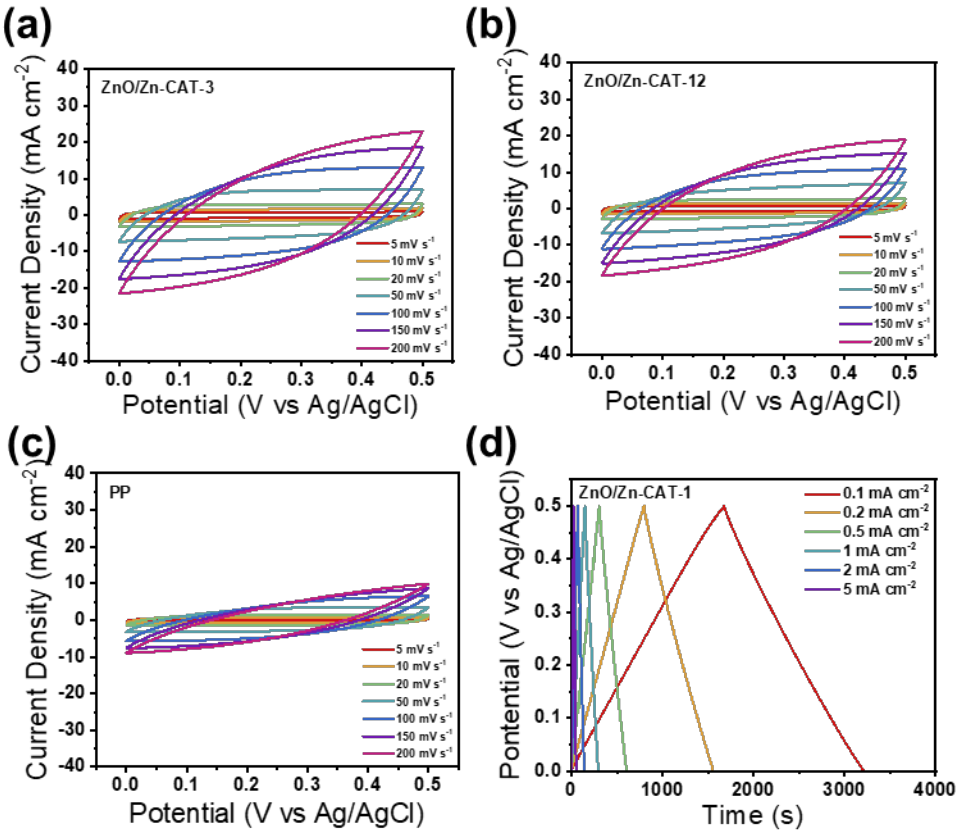

Figure S10. The CV curves of (a) ZnO@Zn-CAT-3/PP, (b) ZnO@Zn-CAT-12/PP, and (c) pure PP electrode at scan rates from 5 to 200 mV s^{-1}; (d) the galvanostatic charge/discharge curves of the ZnO@Zn-CAT-1/PP electrode at current densities from 0.1 to 5 mA cm^{-2}.

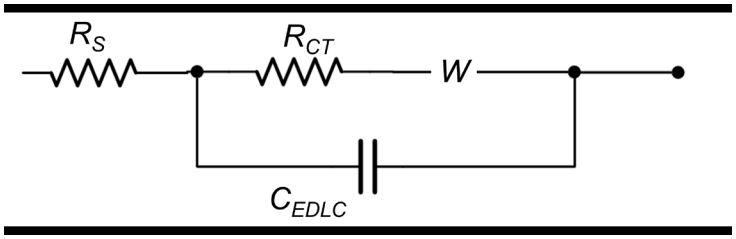

Figure S11. The equivalent circuit model of ZnO@Zn-CAT/PP electrode. where R_S is the equivalent series resistances, R_{CT} corresponds to the charge transfer resistance, which can be measured as the diameter of the semicircle, and *W* represents the finite-length Warburg resistance. C_{EDLC} is electrical double-layer capacitance.

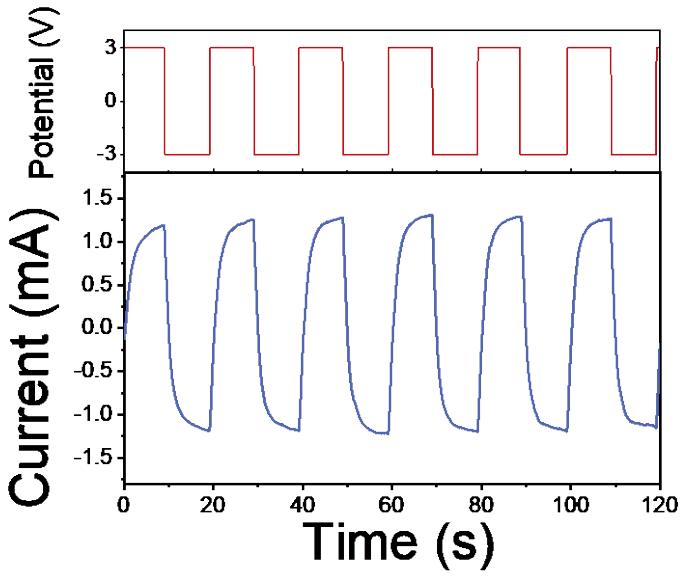

Figure S12. The input voltage signal and current response of ZnO@Zn-CAT-1 based actuator at an applied voltage of ±3.0 V with a frequency of 0.1 Hz.

Tabel S5. Blocking forces

Voltage (V)	ZnO@Zn-CAT-1 soft actuator without light		ZnO@Zn-CAT-1 soft actuator under 700 nm light	
	Average blocking force (mN)	Standard error (mN)	Average blocking force (mN)	Standard error (mN)
0.5	2.4	0.72	3.9	2.3
1	5.3	0.56	14.6	1.3
3	15.9	0.73	66.0	3.0
5	29.2	0.78	53.4	5.9

Table S6. Comparison of actuation performance of ZnO@Zn-CAT-1 based actuator with carbon materials, graphene, and MOF derived actuators.

Materials	Strain (%)	Voltage (V)	Frequency (Hz)	Force (mN)	Response time (s)	Response rate (% s^{-1})	Ref
G-CNT-Ni	0.52	1	0.1	4.53	-		[S1]
pMoS_2-nSNrGO	1.25	0.5	1	6.8	10	0.12	[S2]
Ni-MOFs-700C	0.72	1	0.1	19.8	1.52	0.47	[S3]
NSCOF	0.65	1	0.1	18 gf g^{-1}	2.28	0.29	[S4]
Cu-CAT@MWCNT	0.52	3	0.1	-	50	0.0104	[S5]
Ni-CAT/CNF	0.36	3	0.1	1.45	19	0.019	[S6]
CoNC (x, x = 600-900)	0.28	3	0.1	-	30	0.0093	[S7]
ZnO@Zn-CAT-1	**1.22**	**3**	**0.1**	**15.9**	**1.56**	**0.78**	**This work**
	2.38	**3**	**0.1**	**60**	**1.56**	**1.53**	

References

[S1] J. Kim, S. H. Bae, M. Kotal, T. Stalbaum, K. J. Kim, I. K. Oh, *Small* **2017**, 13.

[S2] M. T. Manzoor, V. H. Nguyen, S. Umrao, J. H. Kim, R. Tabassian, J. E. Kim, I. K. Oh, *Adv. Funct. Mater.* **2019**, 29.

[S3] M. Mahato, W. J. Hwang, R. Tabassian, S. Oh, V. H. Nguyen, S. Nam, J. S. Kim, H. Yoo, A. K. Taseer, M. J. Lee, H. Zhang, T. E. Song, I. K. Oh, *Adv. Mater.* **2022**, 34, e2203613.

[S4] M. Mahato, R. Tabassian, V. H. Nguyen, S. Oh, S. Nam, K. J. Kim, I. K. Oh, *Adv. Funct. Mater.* **2020**, 30.

[S5] Y. Wu, Y.-X. Shi, Y.-Y. Wang, Y.-F. Wang, L.-h. Li, S.-M. Feng, L. Liu, L.-L. Li, T. Li, T. Zhang, *Adv. Mater. Technol.* **2022**, n/a, 2200258.

[S6] Y. X. Shi, Y. Wu, S. Q. Wang, Y. Y. Zhao, T. Li, X. Q. Yang, T. Zhang, *J. Am. Chem. Soc.* **2021**, 143, 4017.

[S7] F. Lu, T. Chen, K. Xiang, Y. Wang, *Polym. Test.* **2020**, 84, 106413.